A Cell Surface Biotinylation Assay to Reveal Membrane-associated Neuronal Cues: Negr1 Regulates Dendritic Arborization*[S]

Francesca Pischedda‡, Joanna Szczurkowska§, Maria Daniela Cirnaru‡, Florian Giesert¶, Elena Vezzoli‖, Marius Ueffing‡‡, Carlo Sala‡, Maura Francolini‖, Stefanie M. Hauck‡‡, Laura Cancedda§, and Giovanni Piccoli‡§§**

A complex and still not comprehensively resolved panel of transmembrane proteins regulates the outgrowth and the subsequent morphological and functional development of neuronal processes. In order to gain a more detailed description of these events at the molecular level, we have developed a cell surface biotinylation assay to isolate, detect, and quantify neuronal membrane proteins. When we applied our assay to investigate neuron maturation *in vitro*, we identified 439 differentially expressed proteins, including 20 members of the immunoglobulin superfamily. Among these candidates, we focused on Negr1, a poorly described cell adhesion molecule. We demonstrated that Negr1 controls the development of neurite arborization *in vitro* and *in vivo*. Given the tight correlation existing among synaptic cell adhesion molecules, neuron maturation, and a number of neurological disorders, our assay results are a useful tool that can be used to support the understanding of the molecular bases of physiological and pathological brain function. ***Molecular & Cellular Proteomics 13: 10.1074/mcp.M113.031716, 733–748, 2014.***

Genetic analysis indicates that 20% to 30% of the total open reading frame encodes for integral membrane proteins (1). Although less abundant than cytosolic proteins, membrane-passing proteins contribute to the regulation of all major cell processes and signaling pathways. In particular, membrane proteins play an important role in the establishment of functional neuronal circuitries during development. This process initially entails the growth, guidance, and stabilization of neuronal processes (axons and dendrites) in a timely, ordered manner involving cell surface molecules that sense the extracellular surroundings and activate signaling cascades (2).

Then, specialized cell-to-cell connections, the synapses, are formed. These connections allow information to flow from one neuron to another and relay the precise juxtaposition and interactions between the pre- and postsynaptic membrane proteins to support their final functional establishment. Several families of synaptic transmembrane or membrane proteins, such as semaphorin, neuroligin, neurexin, and the immunoglobulin superfamily (IgSF),[1] are implicated in neurite formation and synapse establishment (3). However, the picture of membrane proteins expressed in neurons is still far from being completely resolved, and it is expected that many other key molecules are awaiting identification (4). Thus, uncovering the nature of the dynamic multiprotein complexes expressed at the plasma membrane will possibly strongly support the understanding of the mechanism controlling structural and functional neuron development. Here, we describe a biochemical approach to isolate and quantify proteins exposed at the extracellular side of the plasma membrane. Our assay utilized affinity purification on streptavidin resin of biotinylated membrane proteins extracted from a crude synaptosomal preparation. We combined this cell surface biotinylation assay with MS/MS analysis and label-free quantification to investigate protein patterns characterizing immature and mature neuronal cultures. Our analysis identified a panel of 439 differentially expressed proteins, including 109 membrane proteins. In particular, we found that the expression profile of 20 cell adhesion molecules belonging to the IgSF was tightly correlated to neuronal maturation. Among our hits, we focused on Negr1, and we demonstrated that it

From the ‡Institute of Neuroscience CNR, 20129 Milano, Italy; §Istituto Italiano di Tecnologia, 16163 Genova, Italy; ¶Institute of Developmental Genetics, Helmholtz Zentrum München (GmbH), German Research Center for Environmental Health, 85764 Neuherberg, Germany; ‖Department of Medical Biotechnology and Translational Medicine, Università degli Studi di Milano, 20129 Milano, Italy; **Institute for Ophthalmic Research, Eberhard Karls University Tübingen, 72076 Tübingen, Germany; ‡‡Research Unit Protein Science, Helmholtz Zentrum München (GmbH), German Research Center for Environmental Health, 85764 Neuherberg, Germany

Received June 26, 2013, and in revised form, November 22, 2013.
Published, MCP Papers in Press, December 31, 2013, DOI 10.1074/mcp.M113.031716
Author contributions: L.C. and G.P. designed the research; L.C., S.H., and G.P. wrote the manuscript; F.P., J.S., M.D.C., M.F., E.V., S.H., and F.G. performed experiments; M.U., C.S., and S.H. provided data analysis expertise.

[1] The abbreviations used are: IgSF, immunoglobulin superfamily; DIV, days *in vitro*; CAM, cell adhesion molecule; SV, synaptic vesicle; P2, crude synaptosomal pellet; S2, cytosomal supernatant; GO, gene ontology.

plays a key role in regulating neuronal morphological development *in vitro* and *in vivo*.

EXPERIMENTAL PROCEDURES

Lentiviral Vector Constructs, Virus Production, and Plasmids—Negr1 target sequences were identified using Ambion Web-based oligo-search software, and four silencing sequences for Negr1 (A2, 5′-CACCCTTTGATGCTCCATCTT-3′; B1, 5′-AAGATGGAGCATCAAAGGGTG-3′; D4, 5′-AATGTTGATGTAACAGATG-3′; C8, 5′-CTGGAGGCTGTAGTCTCTT-3′) were selected, synthesized, and cloned into GFP-expressing pLVTH, as previously described (5). In brief, oligonucleotides coding for a 5′-pseudoBglII site, a sense-oligonucleotide-loop-antisense-oligonucleotide transcription termination site, and a 3′pseudo-XbaI restriction site were purchased from Metabion, Martinsried, Germany. Sense and antisense oligos were annealed and subsequently phosphorylated. The fragments were cloned 3′ to the H1 promoter of pBC KS+(ClaI)-H1, resulting in pBC KS+(ClaI)-sh. The H1sh cassettes were isolated with ClaI, blunted, and cloned into the blunted ClaI/BamH1 site of pLV transfer vector. pLV is a modified plasmid transfer vector derived from original pLVTH (6) in which the BamH1-tetO-H1-ClaI fragment has been excised. All recombinant lentiviruses were produced by means of transient transfection of HEK293T cells according to standard protocols (6). Primary neuronal cultures were transduced with viruses at multiplicity of infection 1. mNegr1 cDNA (Addgene clone C3342IRCKp5014P057-rzpdm13–21) was cloned into strep-FLAG pcDNA3.1 vector. For rescue experiments, we introduce into mNegr1 cDNA via site-directed mutagenesis two silent mutations in the region targeted by miRNA A2 using the following primer: 5′-GCCGTGGACAACATGCTCGTCAGGAAAGGTGACACAGCG-3′.

Neuronal Cultures—Cortical neuron cultures were prepared from mouse embryos (E17.5–18.5; strain C57BL/*6*). High-density (750 to 1000 cells/mm^2) and medium-density (150 to 200 cells/mm^2) neuronal cultures were plated and grown on six-well plastic tissue culture plates (Iwaki, Bibby Sterilin, Staffordshire, UK) or on 12-mm-diameter coverslips put into 24-well plastic tissue culture plates as previously described (Iwaki, Bibby Sterilin, Staffordshire, UK) (7). In these cultures glial growth is reduced to less than 0.5% of the nearly pure neuronal population (8). Neuronal cultures were infected with viruses at days *in vitro* (DIV) 1 to 2 or transfected at DIV4 with Lipofectamine 2000 following the manufacturer's protocol (Lifetech, Carlsbad, CA).

Cell Surface Biotinylation Assay and Western Blotting—Neurons were incubated at DIV6 or DIV16 with 0.5 mg/ml nonpermeable biotin (NHS-biotin, Sigma-Aldrich) in PBS for 30 min under gentle agitation. After incubation, cells were washed with 100 mM glycine in PBS three times and PBS once, with each washing lasting 10 min.

Subsequently, subcellular fractions were produced as previously described (9). Briefly, high-density cultures were collected in HEPES-buffered sucrose (0.32 M sucrose, 4 mM HEPES pH 7.4) and spun at 600*g* for 5 min to pellet the nuclear fraction. The resulting supernatant was centrifuged at 10,000*g* for 15 min to obtain a cytosolic supernatant (S2) and a crude synaptosomal pellet (P2). The P2 fraction was solubilized in a dedicated lysis buffer (150 mM NaCl, 1% Nonidet P-40, 0.4% n-dodecyl-β-D-maltoside, 0.1% SDS, and 50 mM HEPES, pH 7.4) for 1 h. The lysates from P2 and S2 were spun for 20 min at 16,000*g*, and the supernatant was added to streptavidin-agarose beads and put under mild agitation for 1 h. After the incubation, the resin was washed twice with a wash buffer containing 150 mM NaCl, 50 mM Hepes, 0.1% Triton X-100. A brief centrifugation at 2000*g* followed each wash. Proteins were eluted in 60 μl of 2X Laemmli buffer. To assay protein expression *in vivo*, C57BL/*6* mice were sacrificed when indicated. Cortexes were isolated and homogenized manually in lysis buffer. After 1 h under mild agitation, lysate was clarified by centrifugation for 20 min at 16,000*g*. All procedures described here were performed at 4 °C. The protein concentration in each sample was measured via standard Bradford assay (Bio-Rad). For protein identification and relative quantification via Western blotting, a proper volume of sample containing an equal amount of proteins was diluted with 0.25% 5X Laemmli buffer and loaded onto 4–12% NuPAGE gels (Invitrogen); the proteins were transferred onto nitrocellulose membrane (Sigma-Aldrich) at 80 V for 120 min at 4 °C. The primary antibodies were applied overnight in a blocking buffer (20 mM Tris, pH 7.4, 150 mM NaCl, 0.1% Tween 20, and 5% nonfat dry milk); primary antibodies (source in parentheses) included rabbit anti-NR2A 1:1000, goat anti-Negr1 1:1000 (R&D, Minneapolis, MN), rabbit anti-HSP90 1:1000, rabbit anti-NSF 1:1000, rabbit anti RpS6 1:2000 (Cell Signaling, Danvers, MA), mouse anti-NCAM 1:1000 (BD Biosciences), mouse anti-PSD-95 1:5000 (NeuroMab, Davis, CA), mouse anti-MAP2 1:1000, mouse anti-SNAP-25 1:1000, mouse anti-Synaptophysin 1:1000, mouse anti-syntaxin 1A 1:1000, mouse anti-actin 1:1000, mouse anti-α-tubulin 1:1000 (Sigma-Aldrich), and mouse anti-Na/K ATPase α 1:2000 (10) (a generous gift from Grazia Pietrini, University of Milano). The secondary antibodies (HRP-conjugated anti-mouse, anti-rabbit, or anti-rat) (Jackson ImmunoResearch, Suffolk, UK) were used in a ratio of 1:8000. The signal was detected using an ECL detection system (GE Healthcare). Films were acquired on a GS-800 densitometer (BioRad) calibrated following the manufacturers' instructions, and protein abundance was estimated as a function of the optical density of a specific band quantified by ImageJ software (NIH). Unless otherwise stated, all the other chemicals were purchased from Applichem, GmBH, Darmstadt, Germany.

Electron Microscopy—Specimens from neurons at different DIV were prepared for electron microscopy as previously described (11). Briefly, neuronal cultures were fixed in cacodylate buffered with 3% glutaraldehyde for 12 h and subsequently Epon-embedded. Ultrathin sections were cut, mounted on copper grids, contrasted with uranyl acetate and lead citrate, and observed with an electron microscope (Zeiss EM10 at 60 kV). Electron microscopy images were processed on ImageJ (NIH), and single vesicles and synaptic structures were annotated manually. Throughout the text, *n* refers to the number of neurons measured. For transmission electron microscopy analysis of the P2 fraction, samples were fixed with 2% glutaraldehyde in cacodylate buffer (Na-cacodylate 0.1 M, pH 7.4) and processed for transmission electron microscopy. Briefly, after fixation the samples were post-fixed with osmium tetroxide (2% OsO_4 in 0.1 M cacodylate buffer), rinsed, stained with 1% uranyl acetate in water for 45 min, dehydrated, and embedded in epoxy resin (Epon 812, Electron Microscopy Science, Hatfield, PA). The resin was then baked for 48 h at 60 °C. Thin sections (70 nm) were obtained with an ultramicrotome (Reichert Ultracut E, Leica Microsystems, Heerbrugg, Switzerland). Samples were observed with a Philips CM10 transmission electron microscope at 80 kv, and images were acquired using a Morada Olympus digital camera.

Immunofluorescence and Quantification—For the immunostaining experiments, neurons were fixed in 4% paraformaldehyde and 4% sucrose at room temperature or 100% methanol at −20 °C. Primary and secondary antibodies were applied in GDB buffer (30 mM phosphate buffer, pH 7.4, containing 0.2% gelatin, 0.5% Triton X-100, and 0.8 M NaCl) for two hours at room temperature or overnight at 4 °C. Primary antibodies included goat anti-OPCML 1:500, goat anti-NEGR1 1:500 (R&D), mouse anti-LSAMP 1:1000 (DSHB, Iowa City, Iowa), mouse anti-PSD-95 1:500 (NeuroMab), Alexa phalloidin-546 1:2000 (Invitrogen), rabbit anti-MAP2 1:400 (Millipore, Billerica, MA), and mouse anti-Na/K ATPase α 1:100. GFP-positive neurons were randomly chosen for quantification in at least four independent experiments for each condition. The fluorescence images were acquired using an LSM Zeiss 510 confocal microscope with a Zeiss 63× objective (Karl Zeiss, Jena, Germany) at a resolution of 2048 × 2048

pixels, with a pixel size of 0.098 μm. All the measurements were performed using NeuronStudio. Neurites and dendritic spines were automatically traced and quantified by the software in terms of length, number, and morphology (12, 13). Data were then logged and analyzed in Microsoft Excel.

Exo-endocytotic Assay—The endocytosis assay to monitor synaptic vesicle (SV) recycling was performed as previously described with minor modifications (14, 15). Briefly, rabbit polyclonal antibodies directed against the intravesicular domain of synaptotagmin1 (Synaptic Systems, Goettingen, Germany) were diluted in Tyrode solution (124 mM NaCl, 5 mM KCl, 5 mM $CaCl_2$, 1 mM $MgCl_2$, 30 mM glucose, 25 mM HEPES, pH 7.4) and applied for 5 min at room temperature. After fixation and permeabilization, a synaptophysin counterstain (mouse anti-synaptophysin 1:400, Sigma-Aldrich) was performed to visualize the totality of synaptic vesicles. Images were acquired by means of confocal microscopy, processed, and quantitatively analyzed with ImageJ software, as previously described (16).

Mass Spectrometry—Protein samples derived from cellular fractions before Strep pull-down were processed via filter-aided sample preparation as described elsewhere (17). Samples generated via Strep pull-downs were directly digested on bead after reduction and alkylation and repetitive washes with 6 M urea followed by one wash in 5 M NaCl. The peptides generated by tryptic digests were acidified and then subjected to LC-MS/MS as described elsewhere (18). Briefly, LC-MS/MS analysis was performed on an Ultimate3000 nano-HPLC system (Dionex, Sunnyvale, CA) coupled to an LTQ OrbitrapXL mass spectrometer (Thermo Fisher Scientific) by a nanospray ion source. Tryptic peptides were automatically injected and loaded at a flow rate of 30 μl/min in 95% buffer C (0.5% trifluoroacetic acid in HPLC-grade water) and 5% buffer B (98% actetonitrile and 0.1% formic acid in HPLC-grade water) onto a nano trap column (100 μm inner diameter × 2 cm, packed with Acclaim PepMap100 C18, 5 μm, 100 Å; Dionex). After 5 min, peptides were eluted and separated on the analytical column (75 μm inner diameter × 15 cm, Acclaim PepMap100 C18, 3 μm, 100 Å; Dionex) by a linear gradient from 5% to 40% of buffer B in buffer A (2% acetonitrile and 0.1% formic acid in HPLC-grade water) at a flow rate of 300 nl/min over 120 min. Remaining peptides were eluted by a short gradient from 40% to 100% buffer B in 5 min. The eluted peptides were analyzed by the LTQ OrbitrapXL mass spectrometer. From the high-resolution mass spectrometry prescan with a mass range of 300–1500, the 10 most intense peptide ions were selected for fragment analysis in the linear ion trap, if they exceeded an intensity of at least 200 counts, and if they were at least doubly charged. The normalized collision energy for collision-induced dissociation was set to a value of 35, and the resulting fragments were detected with normal resolution in the linear ion trap. The lock mass option was activated, and the background signal with a mass of 445.12002 was used as the lock mass (19). Every ion selected for fragmentation was excluded for 30 s by means of dynamic exclusion. The acquired spectra were processed and analyzed using Mascot Daemon (V2.4.1) with the following settings: cystein carbamidomethylation as a fixed modification; methionine oxidation and asparagine/glutamine deamidation as variable modifications; and one missed cleavage allowed. Mass tolerances for parent and fragment peptides were set at 10 ppm and 0.6 Da, respectively. The database used was the Ensembl Mouse database (version GRCm38; 51,372 sequences, 23,210,570 residues) For the qualitative analysis, Mascot result files were analyzed by Scaffold software (V4.0.7, Proteome Software Inc., Portland, OR) to validate MS/MS-based peptide and protein identifications. Peptide identifications were accepted if they could be established at greater than 95% probability as specified by the Peptide Prophet algorithm (20). Protein identifications were accepted if they could be established at greater than 99% probability and contained at least two identified unique peptides. Protein probabilities were assigned by the Protein Prophet algorithm (21). Protein and peptide false discovery rates were fixed at 1% and 0.1%, respectively. Proteins that contained similar peptides and could not be differentiated based on MS/MS analysis alone were grouped to satisfy the principles of parsimony. All identified proteins with their respective numbers of uniquely identified peptides are listed in supplemental Table S1. All identified peptides are listed in supplemental Table S2.

For relative quantification based on peptide intensities, three independent biological replicates for each experimental condition were analyzed. The raw files were directly imported into Progenesis Software (version 4.0, Nonlinear Dynamics, Newcastle upon Tyne, UK) and processed as described elsewhere (18). Briefly, profile data of the MS scans and MS/MS spectra were transformed into peak lists with Progenesis LC-MS using a proprietary algorithm and then stored in peak lists comprising *m/z* and abundance values. One sample was set as a reference, and the retention times of the other sample within were aligned (three to five manual landmarks, followed by automatic alignment) to create maximal overlay of the two-dimensional feature maps. Features with only one charge or more than seven charges were masked at this point and excluded from further analysis. Samples were then allocated to experimental groups (DIV6 and DIV16, respectively). For quantification, all unique peptides (with Mascot percolator score ≥ 13) of an identified protein were included and the cumulative abundance for that protein was calculated by summing the abundances of all peptides allocated to the respective protein normalized *versus* the total peptide abundance. No minimal thresholds were set for the method of peak picking or selection of data to use for quantification. Based on the cumulative intensities, a ratio between DIV16 and DIV6 was calculated for each protein and evaluated statistically via *t* test. All identified proteins with their respective cumulated peptide intensities from each sample are listed in supplemental Table S3. Peptide quantification is reported in supplemental Table S4.

In Utero Electroporation—*In utero* electroporation was performed with the standard configuration, as described elsewhere (22). In brief, the day of mating (limited to 4 h in the morning) was defined as embryonic day zero (E0), and the day of birth was defined as postnatal day zero (P0). E15.5 timed-pregnant CD1 mice (Harlan Italy SrL, Correzzana, Italy) were anesthetized with isoflurane (induction, 4%; surgery, 2.5%), and the uterine horns were exposed by laparotomy. The DNA (1 to 2 μg/μl in water) together with Fast Green dye (0.3 mg/ml; Sigma, St. Louis, MO) was injected (5 to 6 μl) through the uterine wall into one of the lateral ventricles of each embryo by a 30-gauge needle (Pic indolor, Grandate, Italy). After the uterine horn had been soaked with a PBS solution, the embryo's head was carefully held between tweezer-type circular electrodes (3-mm diameter, Nepa Gene, Chiba, Japan). For the electroporation, six electrical pulses (amplitude, 30 V; duration, 50 ms; intervals, 1 s) were delivered with a square-wave electroporation generator (CUY21EDIT, Nepa Gene, Ichikawa-City, Chiba, Japan; ECM 830, BTX, Harvard Apparatus, Holliston, MA). After electroporation, the uterine horns were returned into the abdominal cavity and embryos were allowed to continue their normal development.

Real-time Reverse-transcription PCR—Quantitative real-time RT-PCR was performed as previously described (23). In short, RNA extracted by the RNeasy Mini Kit (Qiagen, Hilden, Germany) was reverse transcribed using SuperScript®-VILO (Invitrogen, #11904–018). For quantification of *Negr1* and *Ncam1* transcripts, real-time PCR was performed using the ABI PRISM 7900 Sequence Detection System (Applied Biosystems, Carlsbad, CA) and TaqMan® reaction mixes for murine *Negr1* (Mm01317328_m1, Applied Biosystems), *Ncam1* (Mm01149710_m1, Applied Biosystems), and *Actb* (actin, beta) (NM_007393.1, Applied Biosystems). All samples were measured in

triplicate. The relative expression of endogenous *Negr1* and *Ncam1* was determined via normalization to *Actb* ($2^{-[\Delta Ct]}$).

Statistical Analysis—All data are expressed as means ± S.E. Data were analyzed with an unpaired Student's *t* test (two classes) or ANOVA followed by Tuckey's post hoc test (more than two classes). The number of experiments (*n*) and the level of significance (*p*) are indicated throughout the text.

RESULTS

Cell Surface Biotinylation Assay Allows the Enrichment of Membrane Proteins—Our cell surface biotinylation assay exploits the incubation of living neuronal cultures with nonpermeable biotin moieties to tag protein domains at the extracellular level. To minimize protein internalization, we performed the biotinylation step at 4 °C (24). After extensive washing, we collected via sequential centrifugation a series of biochemical fractions, namely, S1 (mainly containing cell body), S2 (cytosol), and P2 (enriched in synaptosome and mitochondria) (9). Transmission electron microscopy investigation of P2 fractions obtained from DIV6 and DIV16 cultures confirmed that both samples contained a subcellular structure recognizable as the synaptosome (supplemental Fig. S1). After solubilization in dedicated lysis buffer, we immobilized biotinylated proteins from P2 and S2 fractions on a streptavidin-agarose resin. After washing, we eluted the proteins in Laemmli buffer and analyzed the fractions via Western blotting. As *bona fide* examples of proteins located at various cellular compartments, we monitored the biochemical profiles of the synaptic proteins NMDA-R subunit 2A, syntaxin 1A, PSD-95, and NSF (Fig. 1*A*); cytoskeletal components such as MAP2, actin, and tubulin (Fig. 1*B*); and cytosolic proteins such as RpS6 and HSP-90 (Fig. 1*C*) in fractions obtained from DIV16 cultures. Western blot analysis showed that the P2 fraction was enriched in synaptic proteins such as PSD-95 and NSF and was mostly lacking in cytosolic components such as RpS6 and HSP-90; furthermore, we found that NMDA-R subunit 2A was present in the eluate of streptavidin pull-down obtained from the P2 fraction (NMDA in STREP-PD was around 26% of the input; Fig. 1*B*). A similar analysis performed on DIV6 culture produced comparable results (supplemental Fig. S2). To further explore the performance of our assay, we analyzed four biological sources obtained from DIV16 cultures by means of MS/MS spectrometry: total cell lysate, P2 fraction, or STREP-PD fraction resulting from total cell lysate or P2 fraction. We detected 1405 unique proteins, including 155 membrane proteins, in total cell lysate; 710 (147 membrane proteins) in STREP-PD from total cell lysate; 1457 (153 membrane proteins) in the P2 fraction; and 692 (166 membrane proteins) in STREP-PD from P2. In particular, STREP-PD from the P2 fraction was characterized by a peculiar subset of proteins not shared with the P2 fraction (74, 24 membrane proteins) or with STREP-PD from lysate (148, 36 membrane proteins) (Fig. 2*A* and supplemental Tables S1 and S2). When we ranked protein hits in function of the number of unique peptides assigned by MS/MS analysis, we found three membrane proteins in STREP-PD fractions, only one in the P2 fraction, and none in total cell lysate among the top four identifications (Fig. 2*B*). Gene ontology (GO) analysis performed on DAVID Bioinformatics Resources 6.7 (25, 26) indicated that the total cell lysate and P2 fraction included about

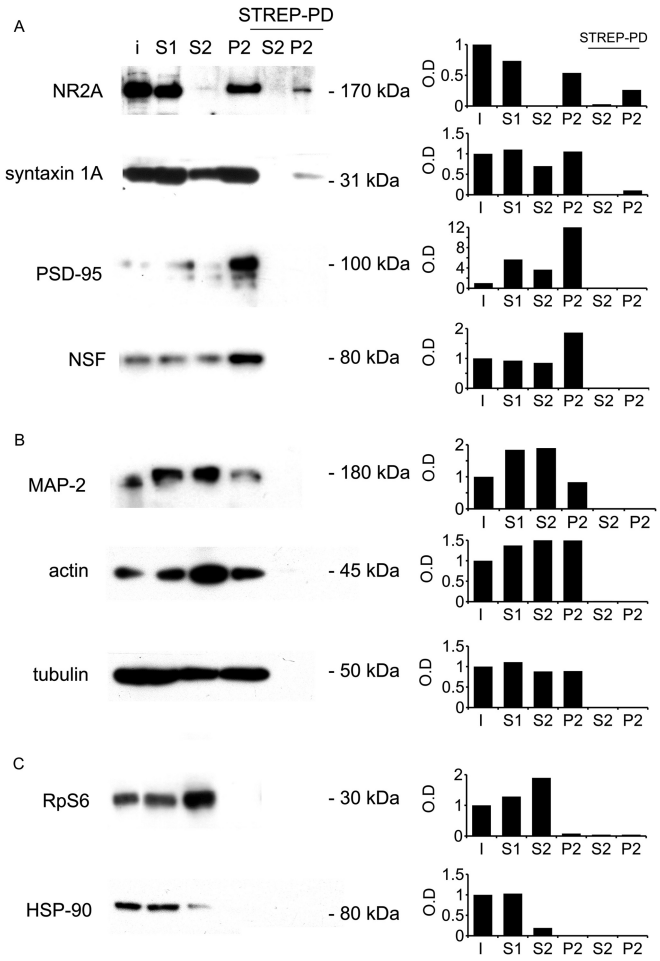

FIG. 1. **Cell surface biotinylation assay isolates membrane proteins.** We developed an assay to enrich our sample in membrane-associated proteins expressed in the synaptosomal fraction. Briefly, cell surface proteins from cortical neurons were biotinylated for 30 min at 4 °C and then processed biochemically to produce input (i, 10% of lysate) and fractions containing nucleus-free supernatant (S1), cytosol (S2), and crude synaptosomes (P2). Biotinylated membrane-associated proteins were eluted in Laemmli buffer after affinity enrichment on Streptavidin resins (STREP-PD). We monitored our protocol via Western blotting with antibodies raised against synaptic (*A*), cytoskeletal (*B*), and cytosolic markers (*C*). Postsynaptic (NMDAR2 subunit NR2A) and presynaptic (syntaxin1A) markers were enriched in the P2 fraction, whereas cytoskeletal (actin and tubulin) or cytosolic proteins (HSP-90) were not present. The left-hand panels show representative blots. For each protein blotted on the left, the histograms on the right report on the *y*-axis the optical density (O.D.) found in each fraction normalized *versus* the input amount. Quantification of the relative abundance of the different proteins in each fraction showed that NR2A was enriched in STREP-PD P2 fraction relative to the other subcellular markers.

A

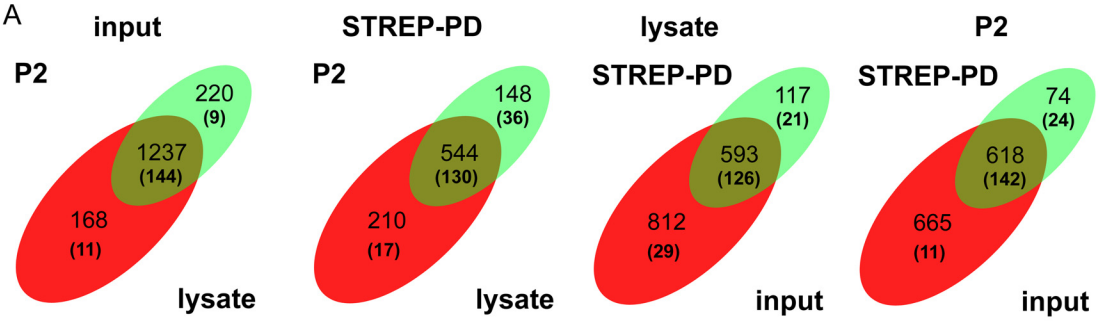

B

Top 4 STREP-PD lysate	Entry	Location	Pep
spectrin beta, non-erythrocytic 1	Q62261	cytoplasm	39
ATPase, Na+/K+ transporting, alpha 3	Q8VCE0	membrane	32
ATPase, Na+/K+ transporting, alpha 3	Q6PIC6	membrane	31
ATPase, Na+/K+ transporting, alpha 1	Q8VDN2	membrane	28

Top 4 STREP-PD P2	Entry	Location	Pep
ATPase, Na+/K+ transporting, alpha 3	Q6PIC6	membrane	29
spectrin beta, non-erythrocytic 1	Q62261	cytoplasm	27
neural cell adhesion molecule 1	P13595	membrane	25
Na+/K+ transporting, alpha 1	Q8VDN2	membrane	23

Top 4 lysate input	Entry	Location	Pep
dynein cytoplasmic 1 heavy chain 1	Q9JHU4	cytoplasm	108
spectrin beta, non-erythrocytic 1	Q62261	cytoplasm	89
clathrin, heavy polypeptide (Hc)	Q68FD5	cytoplasm	62
myosin, heavy polypeptide 10	Q61879	cytoplasm	57

Top 4 P2 input	Entry	Location	Pep
dynein cytoplasmic 1 heavy chain 1	Q9JHU4	cytoplasm	128
spectrin beta, non-erythrocytic 1	Q62261	cytoplasm	87
ankyrin 2, brain	S4R249	membrane	82
clathrin, heavy polypeptide (Hc)	Q68FD5	cytoplasm	62

C

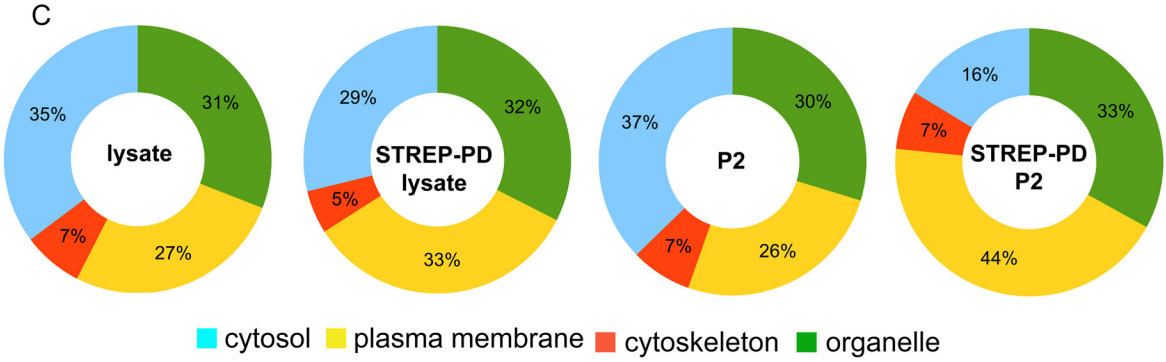

D

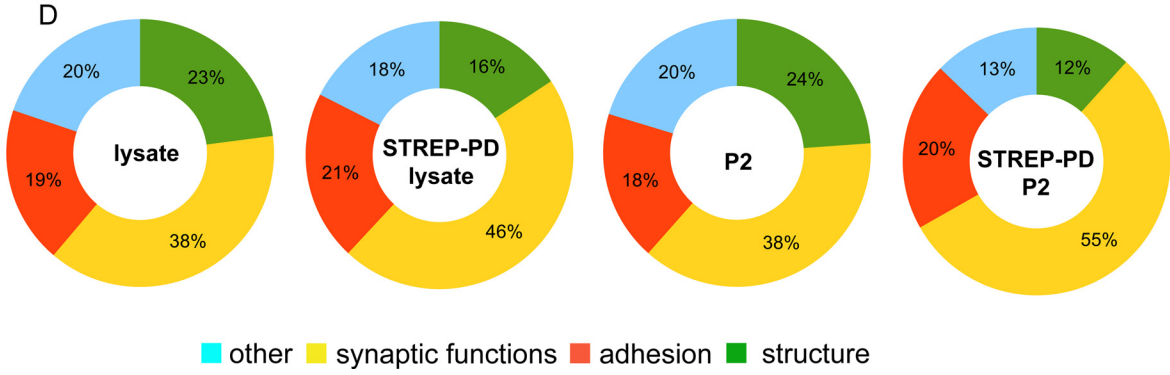

FIG. 2. **Cell surface biotinylation assay isolates membrane proteins involved in synaptic functions.** *A*, Venn diagrams compare the protein datasets identified in total cell lysate and P2 fraction (input), in the STREP-PD fraction obtained from total cell lysate and from P2 (STREP-PD), in STREP-PD from lysate and the lysate itself (lysate), and in STREP-PD from P2 and the P2 fraction itself (P2). "Input" refers to the protein source used in the streptavidin-enrichment procedure. The numbers in parentheses refer to the number of membrane proteins within each fraction. Values reported arose from a combination of four independent experiments. *B*, the tables report the four top entries for total cell lysate, STREP-PD lysate fraction, P2, and STREP-PD P2 fractions based on the number of unique peptides assigned. Protein name, UniProtKB entry, cellular location, molecular weight (MW), number of unique peptides identified (Pep), and sequence coverage (Cov) are indicated. *C*, the graphs report the GO analysis run considering cellular components relative to the proteins identified in total cell lysate, STREP-PD lysate, P2, and STREP-PD P2 fractions. *D*, the graphs report the GO analysis run considering biological processes executed by plasma membrane proteins identified in total cell lysate, STREP-PD lysate, P2, and STREP-PD P2 fractions. Additional information on protein identification, GO annotation, TMHMM prediction, and peptide identification can be found in supplemental Tables S1 and S2.

26% to 27% membrane proteins and that the incubation on streptavidin beads enriched the membrane protein yield by up to 33% and 44% in STREP-PD from total cell lysate and from P2, respectively (Fig. 2*C*). Once we considered the biological functions executed by plasma membrane proteins only, we found that 38% were involved in synaptic functions and about 18% in cell-adhesion-related processes in total cell lysate or the P2 fraction. These fractions rose to 55% and 20% in STREP-PD from P2 (46% and 21%, respectively, in STREP-PD from cell lysate; Fig. 2*D*). In STREP-PD from P2 we listed a number of proteins that had not been previously described at the synaptic site. Thus we considered for further analysis a panel of these hits, namely, Na/K ATPase subunit α, OPCML, and LSAMP. Through immunolocalization assays we were able to confirm their synaptic localization (supplemental Fig. S3). In conclusion, our cell surface biotinylation assay allowed a robust enrichment of membrane proteins. Interestingly, a high percentage of the identified hits were functionally and/or topologically related to the synapse.

Identification of Membrane Proteins Differentially Expressed during Neuronal Development—Membrane proteins play a pivotal role in the functional and structural remodeling experienced by neurons along *in vitro* culturing (27–29). Thus, we assessed the potential of our assay for identifying the membrane-associated proteins involved in neuronal development. In order to profile the main steps characterizing *in vitro* maturation, we analyzed cortical cultures at four different time points (*i.e.* DIV4, DIV8, DIV12, and DIV16) recognized as representative of neuronal maturation (30). Cortical cultures were infected with GFP-expressing viruses (miRNA control; see "Experimental Procedures") at DIV1, fixed, and imaged at DIV4, -8, -12, and -16 (Fig. 3*A* and supplemental Fig. S4*A*).

We measured the neurite number, total length, and complexity (as monitored by Sholl analysis and by the counting of processes for each order of neurite branching; Figs. 3*B*–3*D* and supplemental Fig. S4*B*). The analysis revealed that neurite arborization matured in terms of process number, length, and branching during *in vitro* culturing. To verify whether the structural maturation correlated with functional features, we measured synaptic functions at the four different time points. To this end, we monitored the SV exo-endocytotic rate by exposing cortical living neurons to an anti-synaptotagmin antibody, as previously described (15). Recycling SVs take up the antibody and thus appear as synaptotagmin-positive clusters after fixation and staining (Fig. 3*E*). The quantification of synaptotagmin-positive clusters revealed that the percentage of recycling SVs within the total SV pool increased linearly from DIV4 to DIV16 (Fig. 3*F*). The total vesicle pool estimated via staining with antibodies against an SV integral protein (synaptophysin) after fixation and permeabilization of the cells showed a bimodal profile, with an increase from DIV4 to DIV8 followed by a decrease at DIV12 and a recovery at DIV16 (Fig. 3*G*). This pattern might reveal a process of rapid synaptogenesis followed first by the elimination of unnecessary contacts and later by the establishment of new functional synapses occurring in neuronal networks during physiological development (31). Accordingly, when we examined the neuronal ultrastructure by means of electron microscopy, we noticed that both post- and presynaptic structures changed with *in vitro* culturing, as previously reported (32). In particular, a number of structural parameters such as postsynaptic density, length and width, active zone length, number of SVs in total and docked pools, and SV average diameter increased as culture proceeded *in vitro* (supplemental Fig. S5). In conclusion, we observed major changes when comparing neurons kept in culture until DIV4 with neurons kept until DIV16. Next, we used our biochemical approach to investigate cultures at two time points, DIV6 and DIV16, considered here as archetypes of the immature and mature stages, respectively. We chose DIV6 instead of DIV4 to cope with two opposing issues: the investigation of an early stage and the necessity of collecting a sufficient yield of proteins. Indeed, we noticed from preliminary experiments that we were not able to obtain an amount of proteins sufficient for our analytical purposes from DIV4 culture (data not shown). In order to identify and obtain a semi-quantitative evaluation of the transmembrane protein pattern expressed at synaptic sites in the immature and mature stages, we combined our assay with MS/MS spectrometry and label-free quantification. The analysis revealed 439 proteins differentially expressed between DIV6 and DIV16 (supplemental Tables S3 and S4). With respect to the subcellular localization, 40% of proteins were associated with the plasma membrane (Fig. 4*A* and supplemental Table S3). Functional analysis indicated that 58% of differentially regulated proteins were involved in synaptic functions and 17% in cell–cell adhesion (Figs. 4*B* and 4*C*; supplemental Table S3). Interestingly, among those differentially expressed proteins, we identified 109 transmembrane proteins including 20 cell adhesion molecules (CAMs) belonging to the IgSF (Fig. 4*D*). To support our proteomic evidence, we chose two proteins for further analysis, Negr1 (33, 34) and NCAM-1 (35, 36). Western blotting experiments indicated that Negr1 and NCAM-1 were enriched in the P2 and STREP-PD fractions (Figs. 5*A* and 5*B*) and that they were both present at the synaptic site (Fig. 5*C*). Next we confirmed that Negr1 and NCAM protein expression in both P2 and STREP-PD P2 fractions as well as Negr1 and NCAM mRNAs increased significantly from DIV6 to DIV16 (Figs. 5*D* and 5*E*; quantification in Figs. 5*G*–5*I*). Furthermore, we noticed that Negr1 and NCAM expression in cortex increased during *in vivo* development (Fig. 5*F*; quantification in Fig. 5*J*), whereas the expression of a nonrelated protein, RAB3A, remained constant (supplemental Figs. S6*A* and S6*B*). Thus, our cell biotinylation assay proved to be a valuable tool for investigation of the molecular mechanisms in play during neuronal development.

Negr1 Modulates Neuronal Structural Maturation—Of the differentially expressed CAMs identified in our assay, we fo-

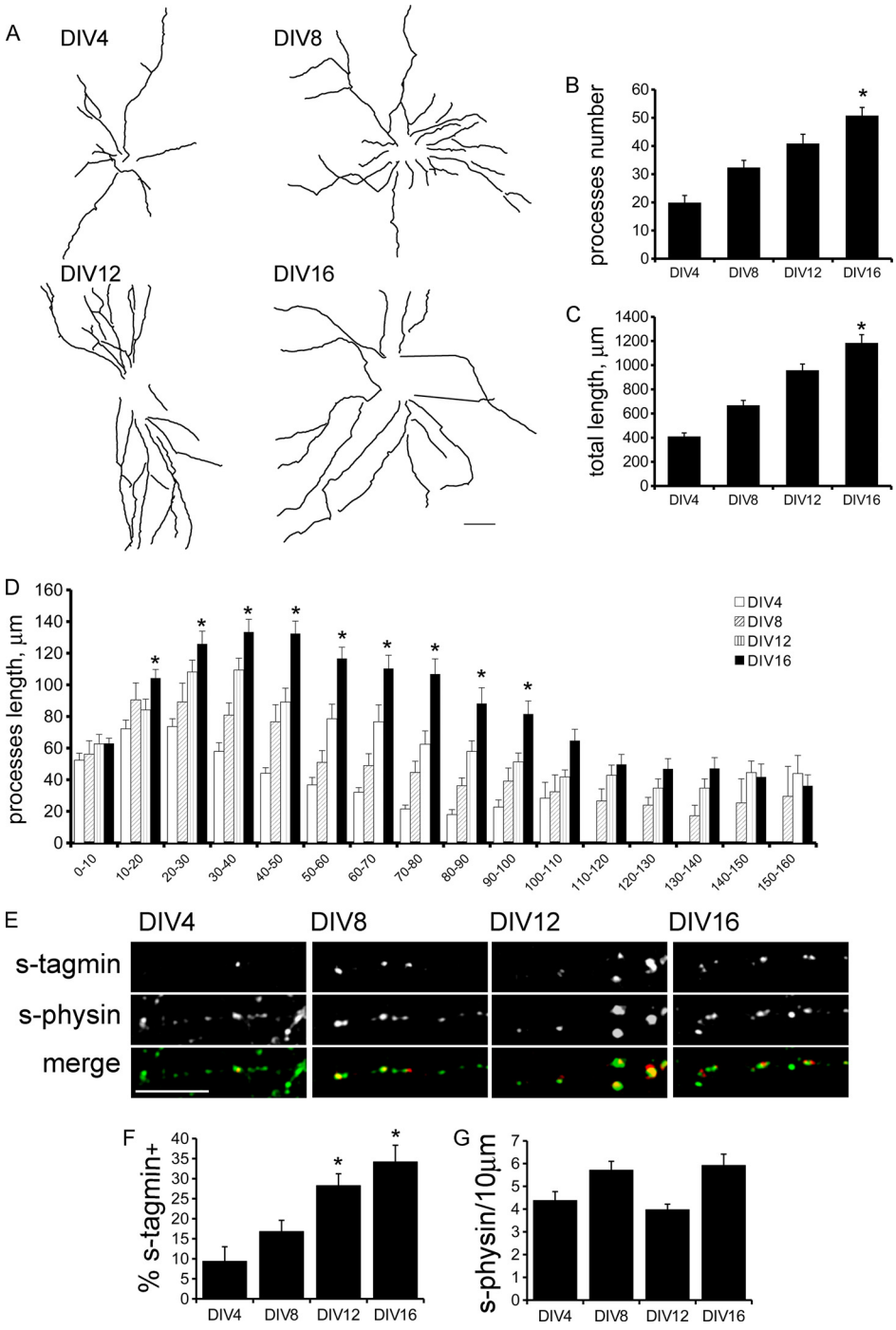

FIG. 3. **Neurons mature anatomically and functionally during *in vitro* culture.** Dissociated cortical cultures were infected at DIV1 with GFP-expressing viruses. At the indicated DIV, cells were fixed and imaged by means of confocal laser microscopy. *A*, *camera lucida* tracing of neurons kept in culture until the indicated DIV. Scale bar = 20 μm. *B*, *C*, quantification of neurite total number and length. *D*, Sholl analysis shows cumulative process length (*y*-axis) in the given spacial bin (in micrometers). Data are expressed as mean ± S.E.; *$p < 0.01$ *versus* DIV4, ANOVA test; $n = 12$ neurons for each experimental case. *E*, the ratios of recycling synapses were estimated in incubating living cortical neurons with anti-synaptotagmin (s-tagmin) antibodies for 5 min before fixation at the indicated DIV. Post-staining with synaptophysin (s-physin) revealed the total number of synapses. Representative images were acquired with a laser-assisted confocal microscope at 63× magnification. During *in vitro* development, neurons mature functionally as indicated by the growing number of actively recycling synapses. Scale bar = 20 μm. *F*, quantification of the ratio of clusters positive for both s-tagmin and s-physin (recycling synapses) expressed as a percentage of s-physin-positive clusters (total number of synapses) in the same section. *G*, total number of s-physin-positive clusters/10 μm. Data are expressed as mean ± S.E.; *$p < 0.05$ *versus* DIV4, ANOVA test; $n = 4$, 10 neurons for each experimental case.

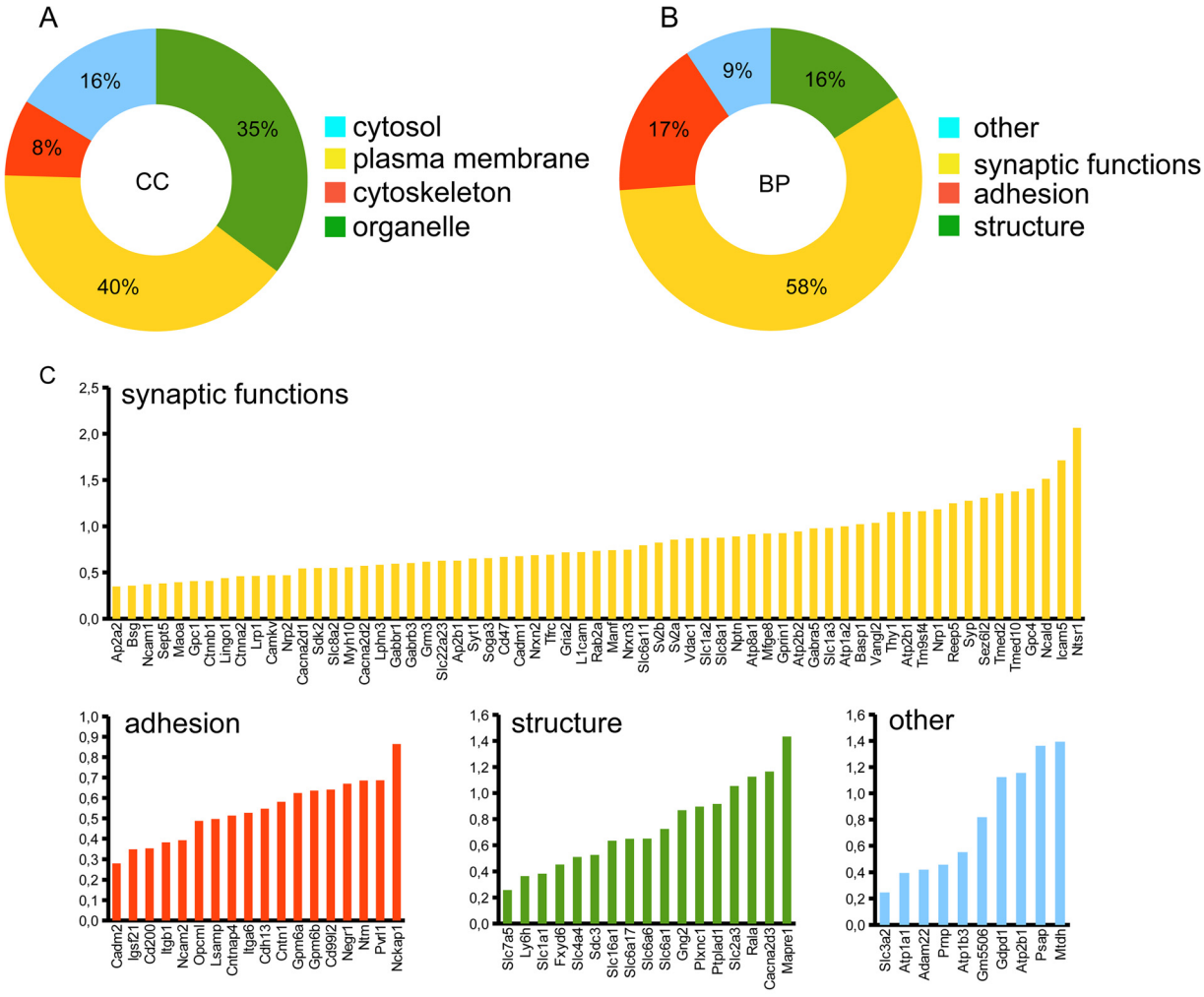

D

Description	gene	div16/div6	T-Test	#	score
basigin	Bsg	2,3	0,008	9	657
CD200 antigen	Cd200	2,3	0,048	3	114
CD47 antigen	Cd47	4,7	0,007	4	342
cell adhesion molecule 1	Cadm1	4,7	0,008	4	306
cell adhesion molecule 2	Cadm2	1,9	0,031	4	233
contactin 1	Cntn1	3,8	0,005	29	2222
immunoglobulin superfamily, member 21	Igsf21	2,2	0,004	2	161
intercellular adhesion molecule 5	Icam5	51,6	0,000	2	79
L1 cell adhesion molecule	L1cam	5,3	0,003	15	923
leucine rich repeat and Ig domain containing 1	Lingo1	2,7	0,032	6	374
limbic system-associated membrane protein	Lsamp	3,1	0,005	7	383
neural cell adhesion molecule 1	Ncam1	2,3	0,037	30	2725
neural cell adhesion molecule 2	Ncam2	2,5	0,008	10	973
neuronal growth regulator 1	Negr1	4,7	0,001	6	351
neuroplastin	Nptn	7,7	0,000	2	284
neurotrimin	Ntm	4,8	0,002	4	445
opioid binding protein/cell adhesion molecule-like	Opcml	3,1	0,004	6	551
poliovirus receptor-related 1	Pvrl1	4,9	0,010	3	322
sidekick homolog 2	Sdk2	3,5	0,001	3	140
thymus cell antigen 1, theta	Thy1	14,2	0,004	3	300

cused on Negr1. Negr1 belongs to a subgroup of the IgSF named IgLON. IgLON CAMs are implicated in synapse formation, functions, and plasticity (37). Given the expression profile we reported for *in vitro* culturing, we investigated the impact of Negr1 on neuronal morphological maturation. To this aim, we generated artificial viruses carrying GFP reporter and an miRNA-like construct able to silence Negr1 expression down to 20% of its endogenous level (supplemental Figs. S6*C*–S6*G*), reducing the short-hairpin RNA-related adverse effect (5). To evaluate the effect of Negr1 silencing on neuronal structure, we infected cortical cultures at DIV1 with viruses carrying miRNA Negr1 or miRNA control and fixed the cells at an immature (DIV6) or mature (DIV16) stage. On these cultures, we measured the neurite number, total length, and complexity (as monitored by Sholl analysis and the count of process number for each order of branching). The analysis revealed that Negr1 down-regulation did not have a significant effect on neurite arborization at DIV6 (Fig. 6). Instead, when we analyzed neurons cultured until DIV16, we found that miRNA Negr1-infected cells were characterized by significantly less complex neuritic trees than culture-matched miRNA control-infected cells (Figs. 7*A* and 7*B*). In particular we noticed that Negr1 silencing induced a decrease in neurites' total length and number (process total length, miRNA control = 1287.6 ± 91.1, miRNA Negr1 = 799.0 ± 77.1; process number, miRNA control = 54 ± 3.7, miRNA Negr1 26.7 ± 3.1; $p < 0.01$; Figs. 7*C* and 7*D*). The staining with antibodies raised against the dendritic protein MAP2 (38) suggested that Negr1 silencing affected mainly dendritic development (supplemental Fig. S7). We obtained comparable results when we down-regulated Negr1 expression via infection with a virus bearing a second Negr1 silencing construct (supplemental Fig. S8). Dendritic spines constitute the main postsynaptic elements of excitatory synapses and are morphologically distinguished as mushroom, stubby, or filopodia-like. Mushroom spines are considered mature and fully functional and are decorated by postsynaptic density markers such as PSD-95 and actin, whereas immature protrusions lack these components (39, 40). Interestingly, a previous report indicated that Negr1 overexpression positively modulates the dendritic spine number, but no evidence on the role of endogenous Negr1 has been provided so far (33). Thus we imaged dendritic protrusions in control and Negr1 silenced neurons at DIV16 and found mature protrusions stained by PSD-95 and actin or filopodial-like structures missing these markers (Fig. 8*A*). Interestingly, when we quantified the number and morphology of dendritic spines, we found that Negr1 silencing decreased the total spine number but did not have a significant impact on the morphology of these structures (spine number/10 μm: miRNA control = 1.9 ± 0.2, miRNA Negr1 = 1.33 ± 0.1, $p < 0.05$; Fig. 8*B*).

Given the implication of Negr1 involvement during neuronal morphological maturation *in vitro*, we verified its role *in vivo*. To this end, we injected miRNA control or miRNA Negr1 into the lateral ventricle of E15.5 mouse *in utero* and electroporated them into a subpopulation of neural progenitors and their progeny. After allowing *in vivo* development, we analyzed the somatosensory cortex in coronal slices obtained from pups at P7. To appreciate neuron morphology, we acquired confocal images of the GFP fluorescence in layer II/III cortical neurons that were derived from miRNA-transfected progenitors (Fig. 9*A* and supplemental Fig. S9*A*). We found that Negr1 miRNA cells displayed reduced basal dendrite arborization relative to controls, as demonstrated by the quantification of total neurite length and number (process total length: miRNA control = 538.8 ± 38.1, miRNA Negr1 = 359.8.0 ± 25.9, $p < 0.01$; process number: miRNA control = 30.4 ± 2.9, miRNA Negr1 15.7 ± 1.5, $p < 0.001$; Figs. 9*B* and 9*C*) and by Sholl analysis (supplemental Fig. S9*B*). Together, these data indicate that Negr1 down-regulation prevents normal morphological development of pyramidal neurons *in vivo*. Overall, our data suggest a critical role for Negr1 in modulating the structural maturation of neurons.

DISCUSSION

The investigation of membrane proteins is a hard task in proteomic investigations because of their low absolute amounts and their mostly hydrophobic nature. Notwithstanding the huge list of synaptosomal proteins generated by high-throughput proteomic studies, the repository of membrane protein remains poorly represented. Recently, Pielot and colleagues generated a meta-database from 12 proteomic publications describing approaches relying on enrichment of membrane fractions from different brain areas (4). The dataset included more than 2000 proteins, of which only 200 (less than 10%) were allocated to the plasma membrane. However, two articles specifically focusing on the investigation of the neuronal membrane subproteome achieved better results. Li and co-workers combined synaptic plasma membrane puri-

Fig. 4. **Identification of synaptic membrane proteins differentially expressed during neuronal development.** The comparison of STREP-PD fractions obtained from neurons at DIV6 and DIV16 via LC-MS/MS followed by label-free quantification revealed 439 differentially expressed proteins. *A*, *B*, the graphs report the GO analysis for the differentially expressed proteins considering cellular components (*A*) and biological processes (*B*). *C*, the graphs list differentially expressed membrane proteins clustered with respect to the indicated biological processes. DIV16/DIV6 ratio is expressed as Log10. *D*, we found a panel of 20 neuronal IgSF CAMs that were differentially expressed. The list reports the protein description, gene name, fold change between DIV16 and DIV6 (DIV16/DIV6), *p* value as computed after *t* test, number of peptides quantified (#), and cumulative Mascot confidence score (score). Additional protein information, including the protein accession number, description, raw abundance, GO, and peptide quantification, can be found in supplemental Tables S3 and S4.

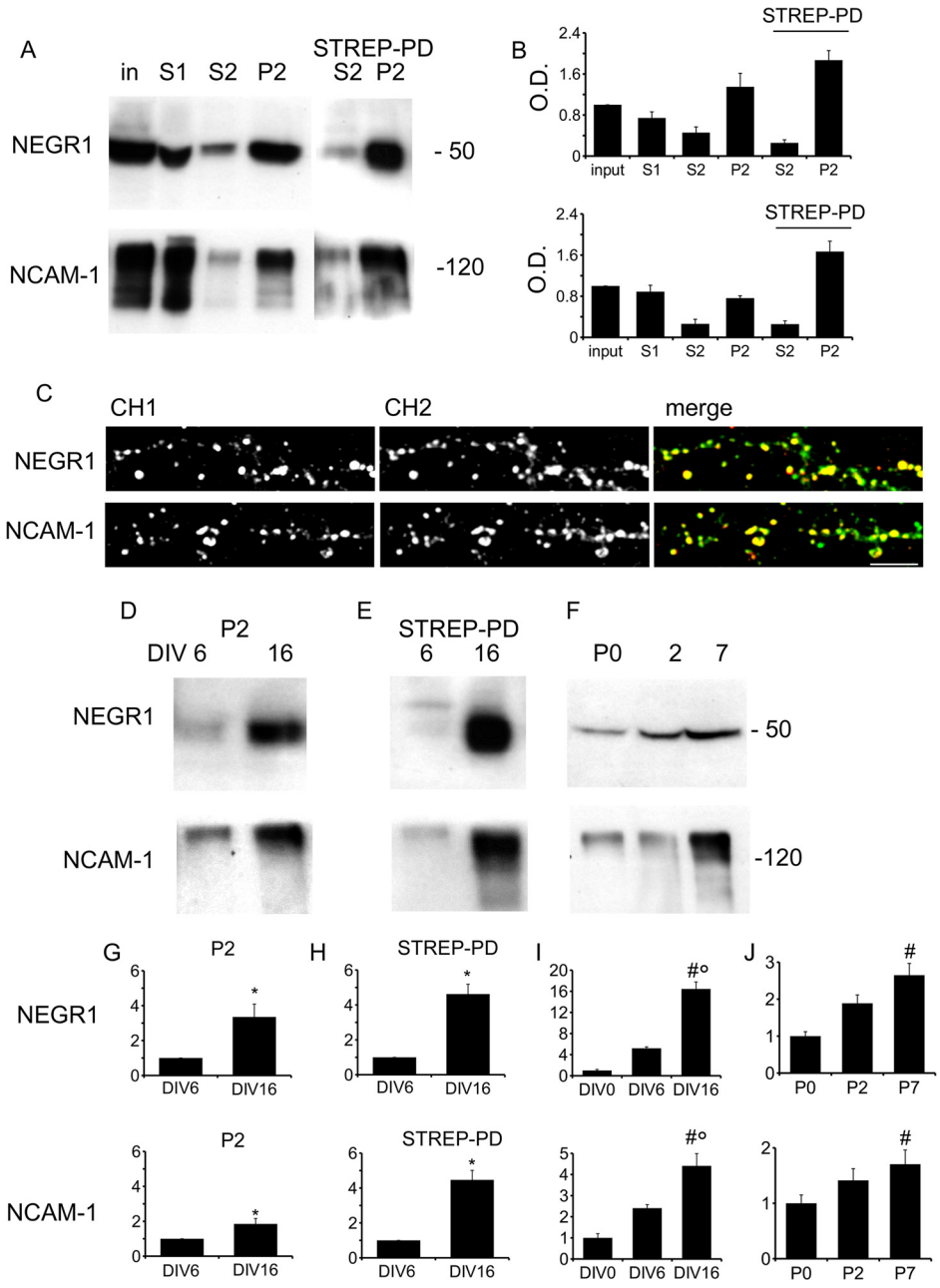

FIG. 5. **Negr1 and NCAM expression increase during *in vitro* and *in vivo* maturation.** *A*, Western blotting analysis of Negr1 and NCAM1 distribution in the biochemical fraction extracted from DIV16 cortical neurons. *B*, the quantification of the relative abundance of Negr1 and NCAM in each fraction normalized *versus* the input amount indicated that Negr1 and NCAM were enriched in STREP-PD obtained from the P2 fraction. *C*, the subcellular localization of Negr1 or NCAM was assayed via staining of DIV16 neuronal cultures with Negr1- or NCAM-specific antibodies (CH1, red) together with antibody against the synaptic marker SV2A (CH2, green). Both Negr1 and NCAM appear as clusters with overlapping with SV2A signals ("merge"). Scale bar = 50 μm. Western blotting analysis of Negr1 expression in P2 (*D*) and STREP-PD from P2 (*E*) obtained from neurons kept in culture until DIV6 and DIV16. *F*, Western blotting analysis of Negr1 expression in lysates obtained from cortexes of mice sacrificed at postnatal day 0 (P0), 2 (P2), or 7 (P7). The panels report the quantification of the relative abundance of Negr1 (upper panels) and NCAM-1 (lower panels) in P2 (*G*) and STREP-PD from P2 fractions (*H*); data were normalized *versus* the DIV6 amount. The analysis confirmed that the expression of Negr1 and NCAM-1 in P2 total and STREP-PD fractions increased during *in vitro* maturation. *I*, primary cortical neurons (DIV0 to DIV16) were analyzed by means of quantitative real-time RT-PCR for Negr-1 (upper) and Ncam-1 (lower) mRNA levels. Relative gene expression was normalized to beta-actin (ACTB) as a housekeeping gene. Expression for DIV0 was set at 1. Data are expressed as mean ± S.E.; # $p < 0.05$ *versus* DIV0, ° $p < 0.05$ *versus* DIV6 $n = 3$. Each sample was measured in triplicate. *J*, quantification of protein amount in postnatal cortices showed that the expression of Negr1 (above) and NCAM-1 (below) increased during *in vivo* maturation. Data were normalized *versus* the P0 amount. Samples containing equal amounts of proteins were resolved by means of SDS-PAGE. Data are based on protein optical density normalized as declared and expressed as mean ± S.E.; Student's *t* test, * $p < 0.05$ *versus* DIV6 or ANOVA # $p < 0.05$ *versus* P0, $n = 4$.

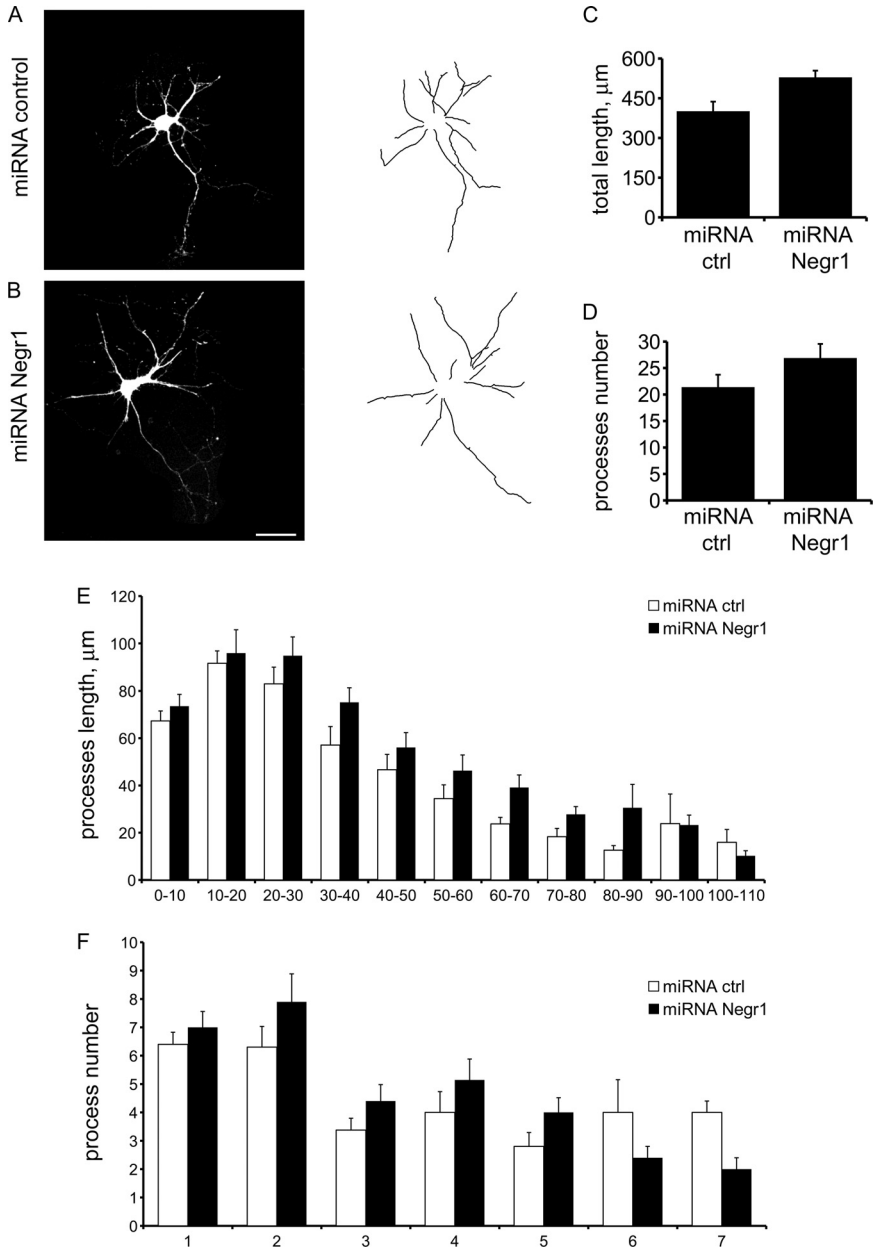

FIG. 6. **Negr1 silencing does not affect neuronal morphology at immature stages.** Cortical neurons were infected at DIV1 with miRNA control and miRNA Negr1. At DIV6, cells were fixed and imaged by means of confocal laser microscopy. *A*, *B*, confocal images highlighting the morphology of neurons infected with miRNA control and miRNA Negr1. Their relative tracings are reported on the right. *C*, *D*, quantification of the neurite total length and number for each neuron. *E*, Sholl analysis shows that Negr1 silencing did not induce significant modification of neurite immature neuronal arborization. *F*, the graph reports the number of neurites in each branching order. Scale bar = 20 μm. Data are expressed as mean ± S.E.; n = 4; 10 neurons were measured for each experimental case.

fication from rat hippocampi with blue native/SDS-PAGE and MS/MS analysis to describe 185 membrane proteins (about 36%) within a database of 514 (41). Additionally, Olsen and colleagues identified 197 membrane proteins (about 35% of 555 total hits) in plasma membrane preparations obtained from different mouse brain areas investigated by means of cation-exchange chromatography coupled with LC-MS/MS (42). In contrast to the approaches described so far in which brain tissue was used as a protein source, we applied cell surface biotinylation on primary neuronal cultures. Primary cultures constitute a robust model to recapitulate neuron physiology and ensure easy access for pharmacological and genetic manipulations that might be difficult, if not impossible, to perform in the intact brain. Furthermore, neurons can be cultured for up to 3 weeks, thus allowing the investigation of dynamic molecular modifications in a time-dependent manner. Our assay fostered the identification of up to 166 membrane proteins. Nevertheless, we found a certain amount of cytosolic/nonmembrane proteins in our dataset. The presence of cytosolic contaminants might have been due to unspecific binding to the agarose matrix of such molecules, characterized by a higher absolute cellular abundance and better solubility in aqueous buffer than membrane-passing molecules. In spite of this technical issue, the performance of our protocol far exceeds the results of similar investigations on primary cultures, to the best of our knowledge. In particular, Stella and colleagues identified about 30 membrane proteins from a preparation of membrane obtained from pri-

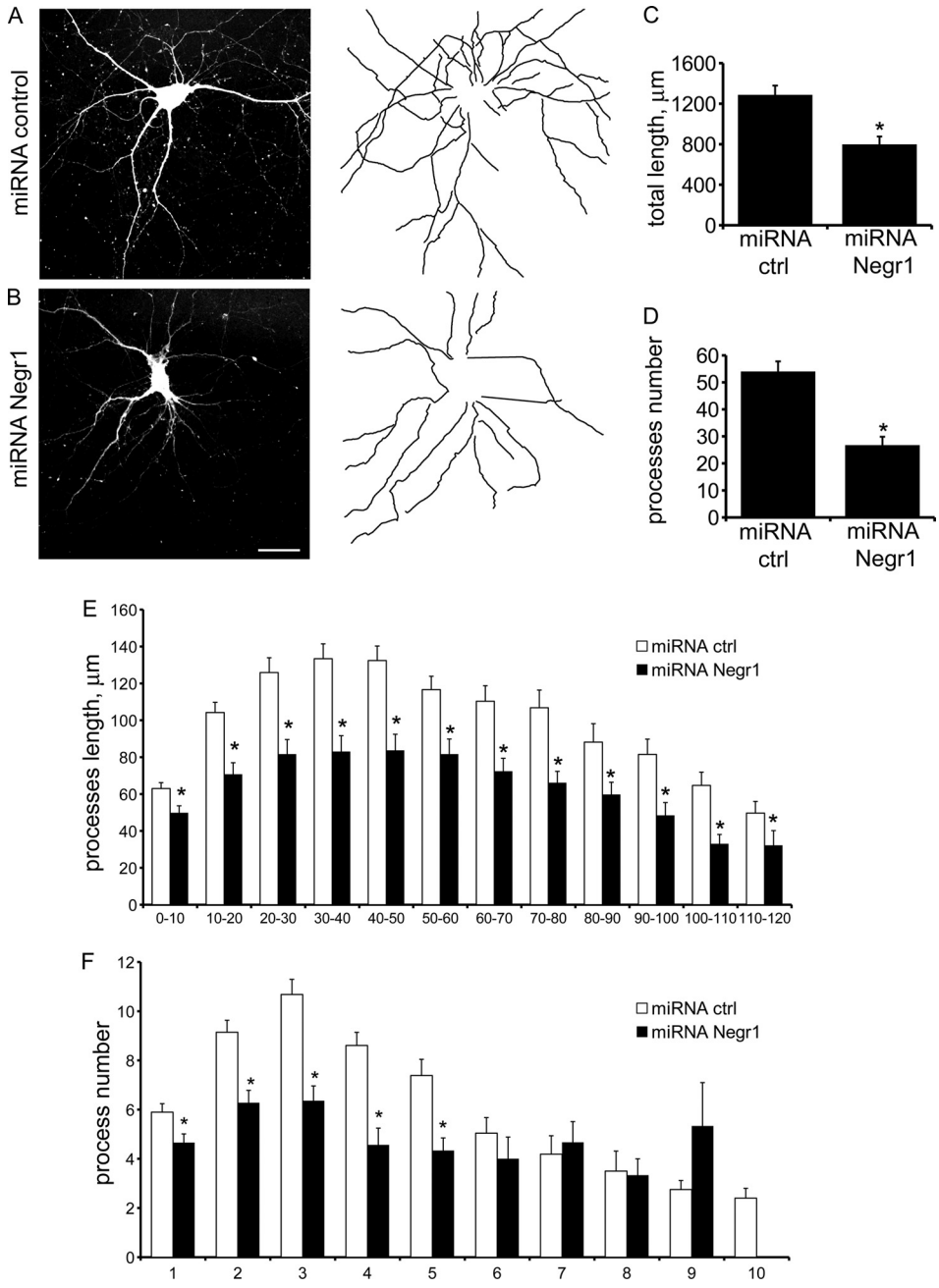

FIG. 7. **Negr1 silencing affects neuronal morphology at mature stages.** Cortical neurons were infected at DIV1 with miRNA control and miRNA Negr1. At DIV16, cells were fixed and imaged by means of confocal laser microscopy. *A*, *B*, morphology of neurons infected with miRNA control and miRNA Negr1 and relative tracing. *C*, *D*, quantification of neurite total length and number for each neuron. *E*, Sholl analysis showed that the neurite arborization was severely affected by miRNA Negr1 infection. *F*, miRNA Negr1 infection altered the distribution of neurites in each branching order. Scale bar = 20 μm. Data are expressed as mean ± S.E.; Student's *t* test, * $p < 0.01$, $n = 4$; 10 neurons were measured for each experimental case.

mary cultures of cerebellar granule neurons (43). The protocol we proposed here implies incubation with nonpermeable biotin with the aim of tagging the proteins truly exposed to the extracellular side at a given functional/developmental stage. Chen and colleagues developed a similar approach and revealed 27 proteins predicted to have at least one transmembrane domain in primary hippocampal cultures (44). Their method lacked the biochemical fractionation utilized here. This difference may account for the much higher recovery of membrane proteins we reported here in comparison to the results of Chen and colleagues. Furthermore, the P2 fraction used in our assay enriches plasma membranes and synaptosome (see supplemental Fig. S1 and Ref. 9), an artificial organelle comprising pre- and postsynaptic elements (45).

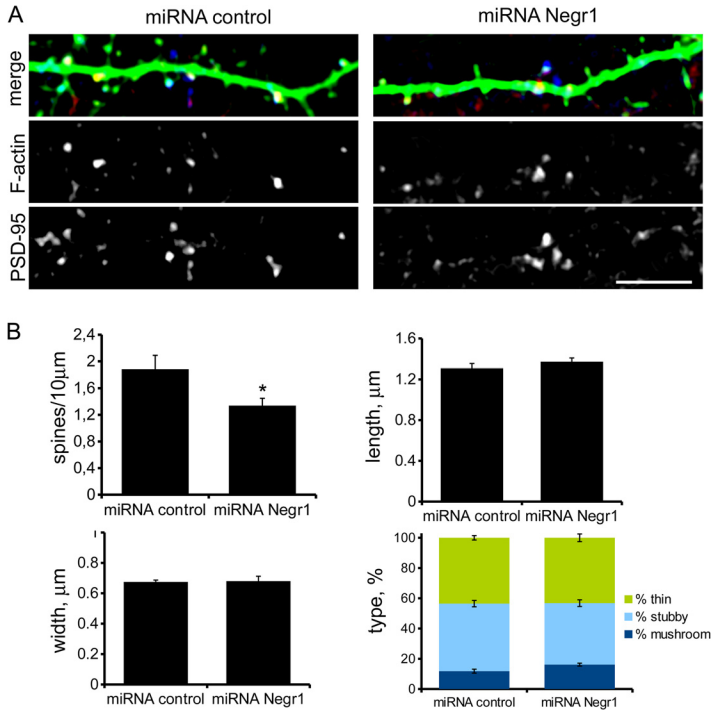

FIG. 8. **Negr1 silencing affects dendritic spine density.** Cortical neurons were infected at DIV1 with miRNA control and miRNA Negr1. At DIV16, cells were fixed, stained, and imaged by means of confocal laser microscopy. *A*, we imaged neuron processes (green) to highlight dendritic spines. Mature spines were decorated by F-actin (red) and PSD-95 (blue). *B*, quantification of morphological parameters describing spines. The panel reports spine density (spine number/10 μm), length, width, and percentage of protrusions characterized by a mushroom, stubby, or thin morphology (type). Scale bar = 10 μm. Data are expressed as mean ± S.E.; Student's *t* test, * $p < 0.05$, $n = 3$; seven neurons were measured for each experimental case.

Accordingly, about 55% of the membrane protein identified by our assay is synaptic or associated with synaptic function according to the GO annotation.

When we compared immature *versus* mature neuronal cultures, we identified a panel of 439 differentially expressed proteins. Among them, we found 109 proteins localized at the plasma membrane, and in particular we found 20 IgSF CAMs. Neuronal IgSF CAMs associate at the cell surface to form homo- and heterophilic complexes and regulate neurite outgrowth and synaptic-contact formation (3). The expression levels of Thy-1 (46), cell adhesion molecule 3 (47), cell adhesion molecule L1 (48), NrCAM (49, 50), neuroplastins (51), and basigin (52) are necessary for the proper establishment of functional neuronal circuitry. Thus, our data are perfectly in line with the fact that the above-mentioned CAMs have a precise expression profile tightly correlated to neuronal maturation. Given their pivotal role during neuronal development, several CAMs have been not surprisingly implicated in neurological disorders (53–55). Recent genetic linkages have associated NrCAM and Negr1 with autism spectrum disorder (56–58).

Negr1 is a synaptic adhesion protein member of the IgLON CAM family (59). In dissociated neurons in culture, Negr1 is mainly observed at axons and presynaptic terminals at early culture stages, but it becomes also postsynaptic at late culture stages (33). Finally, Negr1 overexpression affects the number of synapses with different outcomes depending on the culture stage. If it occurs in early stages, the overexpression of Negr1 decreases the number of synapses, whereas at later stages it is positively associated with synapse number (37). The silencing approach described here sheds light on the physiological function of endogenous Negr1. In particular, we demonstrated that Negr1 hypoexpression induced a significant decrease in the number and length of neuronal processes in mature neurons, thus causing a severe reduction of the overall complexity of neurite arborization *in vitro* and *in vivo*. Given that we reported a similar phenotype in cells overexpressing Negr1, overall our data demonstrate that the Negr1 expression level is tightly associated with neuronal maturation and that it controls the proper development of neurite arborization and dendritic spines.

The pattern of dendrite arborization exhibited by a neuron is tightly correlated to its function. Any alteration in dendrite morphology has dramatic consequences for the proper formation and functionality of the connectivity network within surrounding cells (60, 61). Recent findings point to altered brain connectivity as a key feature in autism spectrum disorder (62). Interestingly, evidence links the pathogenesis of autism spectrum disorder specifically to neuronal-network anomalies and dendritic spine dysmorphology (63–65). We hypothesize that Negr1 regulates the development, formation, and stabilization of a functional neurite network, and consequently Negr1 mutation might contribute to the anatomical aberrations reported in autism spectrum disorder. Independent approaches are needed to confirm the precise localization of the hits identified. Nevertheless, we are confident that our assay can increase the recovery of membrane proteins and facilitate the isolation of molecules functionally and/or topologically related to the synapse.

Finally, our study allowed the preliminary identification of a panel of membrane proteins whose expression was correlated with neuronal development. Although further studies

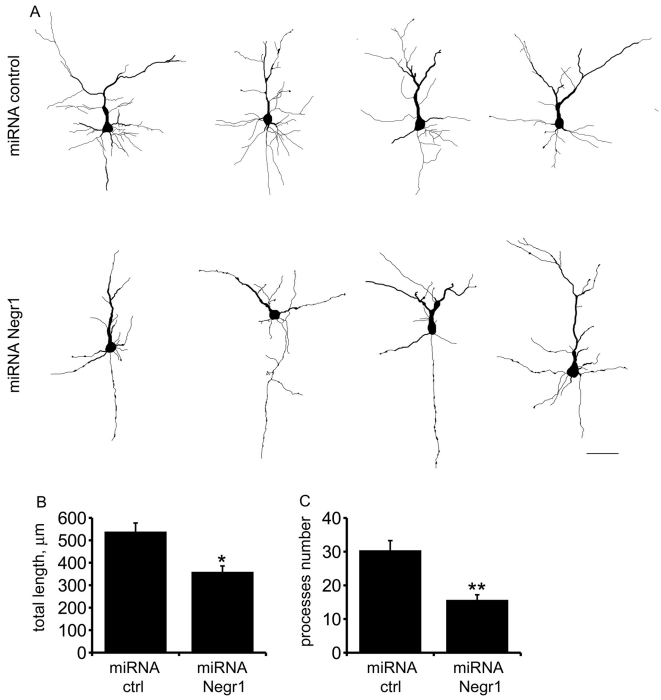

FIG. 9. **Negr1 affects neuronal morphology *in vivo*.** Mouse embryos were electroporated *in utero* at E15.5 with miRNA control or miRNA Negr1 and sacrificed at P7. *A*, *camera lucida* drawing elaborated from confocal images of GFP fluorescence in coronal sections of mouse somatosensory cortices. Negr1 down-regulation resulted in a decrease in the total length (*B*) and number (*C*) of neurite processes. Scale bar = 20 μm; Student's *t* test, * $p < 0.01$, ** $p < 0.001$, $n = 3$; 10 electroporated cells were measured for each experimental case.

will be required to clarify in detail the mechanisms orchestrated by these molecules, our assay proved to be a reliable starting point to study the extracellular proteome and monitor its implication in physiological and pathological neuronal mechanisms.

Acknowledgments—We are grateful to Dr. Ugo Cavallaro (IFOM, Milano, Italy) for reagents and critical discussion.

* This work was supported by the LRRK2 Biology LEAPS program of the Michael J. Fox Foundation (G.P. and M.U.). G.P. is supported by Fondazione Cariplo (Grant No. 2011–0540), the FIRB program (Grant No. RBFR08F82X_002), and Fondazione Telethon (Grant No. GGP12237). L.C. is grateful to the FIRB program (FIRB Grant No. RBFR08F82X). This work was supported by the EU grant 'Systems Biology of Stem Cells and Reprogramming' (SyBoSS [FP7-Health-F4-2010-242129]) and by the Helmholtz Alliance HelMA–Helmholtz Alliance for Mental Health in an Ageing Society, through the Initiative and Network Fund of the Helmholtz Association and (in part) by the Helmholtz Portfolio Theme 'Supercomputing and Modelling for the Human Brain' (SMHB) to F.G.

S This article contains supplemental material.

§§ To whom correspondence should be addressed: Giovanni Piccoli, Institute of Neuroscience, National Research council, IN-CNR Milano, via Vanvitelli 32, 20129 Milano, Italy. Tel.: 390250317093; Fax: 39-0250317132; E-mail: giovanni.piccoli@in.cnr.it.

REFERENCES

1. Wallin, E., and von Heijnbh, E. G. (1998) Genome-wide analysis of integral membrane proteins from eubacterial, archaean, and eukaryotic organisms. *Protein Sci.* **7,** 1029–1038
2. Gerrow, K., and El-Husseini, A. (2006) Cell adhesion molecules at the synapse. *Front. Biosci.* **11,** 2400–2419
3. Maness, P. F., and Schachner, M. (2007) Neural recognition molecules of the immunoglobulin superfamily: signaling transducers of axon guidance and neuronal migration. *Nat. Neurosci.* **10,** 19–26
4. Pielot, R., Smalla, K.-H., Müller, A., Landgraf, P., Lehmann, A.-C., Eisenschmidt, E., Haus, U.-U., Weismantel, R., Gundelfinger, E. D., and Dieterich, D. C. (2012) SynProt: a database for proteins of detergent-resistant synaptic protein preparations. *Front. Synaptic Neurosci.* **4,** 1
5. Bauer, M., Kinkl, N., Meixner, A., Kremmer, E., Riemenschneider, M., Förstl, H., Gasser, T., and Ueffing, M. (2009) Prevention of interferon-stimulated gene expression using microRNA-designed hairpins. *Gene Ther.* **16,** 142–147
6. Wiznerowicz, M., and Trono, D. (2003) Conditional suppression of cellular genes: lentivirus vector-mediated drug-inducible RNA interference. *J. Virol.* **77,** 8957–8961
7. Piccoli, G., Verpelli, C., Tonna, N., Romorini, S., Alessio, M., Nairn, A. C., Bachi, A., and Sala, C. (2007) Proteomic analysis of activity-dependent synaptic plasticity in hippocampal neurons. *J. Proteome Res.* **6,** 3203–3215
8. Brewer, G. J., Torricelli, J. R., Evege, E. K., and Price, P. J. (1993) Optimized survival of hippocampal neurons in B27-supplemented Neurobasal, a new serum-free medium combination. *J. Neurosci. Res.* **35,** 567–576
9. Corti, V., Sanchez-Ruiz, Y., Piccoli, G., Bergamaschi, A., Cannistraci, C. V., Pattini, L., Cerutti, S., Bachi, A., Alessio, M., and Malgaroli, A. (2008) Protein fingerprints of cultured CA3-CA1 hippocampal neurons: comparative analysis of the distribution of synaptosomal and cytosolic proteins. *BMC Neurosci.* **9,** 36
10. Pietrini, G., Matteoli, M., Banker, G., and Caplan, M. J. (1992) Isoforms of the Na,K-ATPase are present in both axons and dendrites of hippocampal neurons in culture. *Proc. Natl. Acad. Sci. U.S.A.* **89,** 8414–8418
11. Rudelius, M., Osanger, A., Kohlmann, S., Augustin, M., Piontek, G., Heinzmann, U., Jennen, G., Russ, A., Matiasek, K., Stumm, G., and Schlegel, J. (2006) A missense mutation in the WD40 domain of murine Lyst is linked to severe progressive Purkinje cell degeneration. *Acta Neuropathol.* **112,** 267–276
12. Wearne, S. L., Rodriguez, A., Ehlenberger, D. B., Rocher, A. B., Henderson, S. C., and Hof, P. R. (2005) New techniques for imaging, digitization and analysis of three-dimensional neural morphology on multiple scales. *Neuroscience* **136,** 661–680
13. Rodriguez, A., Ehlenberger, D. B., Dickstein, D. L., Hof, P. R., and Wearne, S. L. (2008) Automated three-dimensional detection and shape classification of dendritic spines from fluorescence microscopy images. *PLoS One* **3,** e1997
14. Matteoli, M., Takei, K., Perin, M. S., Sudhof, T. C., and De Camilli, P. (1992) Exo-endocytotic recycling of synaptic vesicles in developing processes of cultured hippocampal neurons. *J. Cell Biol.* **117,** 849–861
15. Piccoli, G., Condliffe, S. B., Bauer, M., Giesert, F., Boldt, K., De Astis, S., Meixner, A., Sarioglu, H., Vogt-Weisenhorn, D. M., Wurst, W., *et al.* (2011) LRRK2 controls synaptic vesicle storage and mobilization within the recycling pool. *J. Neurosci.* **31,** 2225–2237
16. Verderio, C., Coco, S., Rossetto, O., Montecucco, C., and Matteoli, M. (1999) Internalization and proteolytic action of botulinum toxins in CNS neurons and astrocytes. *J. Neurochem.* **73,** 372–379
17. Wiśniewski, J. R., Zougman, A., Nagaraj, N., and Mann, M. (2009) Universal sample preparation method for proteome analysis. *Nat. Methods* **6,** 359–362
18. Hauck, S. M., Dietter, J., Kramer, R. L., Hofmaier, F., Zipplies, J. K., Amann, B., Feuchtinger, A., Deeg, C. A., and Ueffing, M. (2010) Deciphering membrane-associated molecular processes in target tissue of autoimmune uveitis by label-free quantitative mass spectrometry. *Mol. Cell. Proteomics* **9,** 2292–2305
19. Olsen, J. V. (2005) Parts per million mass accuracy on an Orbitrap mass spectrometer via lock mass injection into a C-trap. *Mol. Cell. Proteomics* **4,** 2010–2021
20. Keller, A., Nesvizhskii, A. I., Kolker, E., and Aebersold, R. (2002) Empirical statistical model to estimate the accuracy of peptide identifications made by MS/MS and database search. *Anal*. **74,** 5383–5392

21. Nesvizhskii, A. I., Keller, A., Kolker, E., and Aebersold, R. (2003) A statistical model for identifying proteins by tandem mass spectrometry. *Anal*. **75,** 4646–4658
22. dal Maschio, M., Ghezzi, D., Bony, G., Alabastri, A., Deidda, G., Brondi, M., Sato, S. S., Zaccaria, R. P., Di Fabrizio, E., Ratto, G. M., and Cancedda, L. (2012) High-performance and site-directed in utero electroporation by a triple-electrode probe. *Nat. Commun.* **3,** 960
23. Giesert, F., Hofmann, A., Bürger, A., Zerle, J., Kloos, K., Hafen, U., Ernst, L., Zhang, J., Vogt-Weisenhorn, D. M., and Wurst, W. (2013) Expression analysis of Lrrk1, Lrrk2 and Lrrk2 splice variants in mice. *PLoS One* **8,** e63778
24. Sims, K. D., Straff, D. J., and Robinson, M. B. (2000) Platelet-derived growth factor rapidly increases activity and cell surface expression of the EAAC1 subtype of glutamate transporter through activation of phosphatidylinositol 3-kinase. *J. Biol. Chem.* **275,** 5228–5237
25. Huang, D. W., Sherman, B. T., and Lempicki, R. A. (2009) Bioinformatics enrichment tools: paths toward the comprehensive functional analysis of large gene lists. *Nucleic Acids Res.* **37,** 1–13
26. Huang, D. W., Sherman, B. T., and Lempicki, R. A. (2009) Systematic and integrative analysis of large gene lists using DAVID bioinformatics resources. *Nat. Protoc.* **4,** 44–57
27. Higgins, D., Burack, M., Lein, P., and Banker, G. (1997) Mechanisms of neuronal polarity. *Curr. Opin. Neurobiol.* **7,** 599–604
28. Craig, A. M., Jareb, M., and Banker, G. (1992) Neuronal polarity. *Curr. Opin. Neurobiol.* **2,** 602–606
29. Craig, A. M., and Banker, G. (1994) Neuronal polarity. *Annu. Rev. Neurosci.* **17,** 267–310
30. Dotti, C. G., Sullivan, C. A., and Banker, G. A. (1988) The establishment of polarity by hippocampal neurons in culture. *J. Neurosci.* **8,** 1454–1468
31. Trachtenberg, J. T., Chen, B. E., Knott, G. W., Feng, G., Sanes, J. R., Welker, E., and Svoboda, K. (2002) Long-term in vivo imaging of experience-dependent synaptic plasticity in adult cortex. *Nature* **420,** 788–794
32. Mozhayeva, M. G., Sara, Y., Liu, X., and Kavalali, E. T. (2002) Development of vesicle pools during maturation of hippocampal synapses. *J. Neurosci.* **22,** 654–665
33. Hashimoto, T., Yamada, M., Maekawa, S., Nakashima, T., and Miyata, S. (2008) IgLON cell adhesion molecule Kilon is a crucial modulator for synapse number in hippocampal neurons. *Brain Res.* **1224,** 1–11
34. Schäfer, M., Bräuer, A. U., Savaskan, N. E., Rathjen, F. G., and Brümmendorf, T. (2005) Neurotractin/kilon promotes neurite outgrowth and is expressed on reactive astrocytes after entorhinal cortex lesion. *Mol. Cell. Neurosci.* **29,** 580–590
35. Gascon, E., Vutskits, L., and Kiss, J. Z. (2007) Polysialic acid-neural cell adhesion molecule in brain plasticity: from synapses to integration of new neurons. *Brain Res. Rev.* **56,** 101–118
36. Durbec, P., and Cremer, H. (2001) Revisiting the function of PSA-NCAM in the nervous system. *Mol. Neurobiol.* **24,** 53–64
37. Hashimoto, T., Maekawa, S., and Miyata, S. (2009) IgLON cell adhesion molecules regulate synaptogenesis in hippocampal neurons. *Cell Biochem. Funct.* **27,** 496–498
38. Caceres, A., Binder, L. I., Payne, M. R., Bender, P., Rebhun, L., and Steward, O. (1984) Differential subcellular localization of tubulin and the microtubule-associated protein MAP2 in brain tissue as revealed by immunocytochemistry with monoclonal hybridoma antibodies. *J. Neurosci.* **4,** 394–410
39. Bosch, M., and Hayashi, Y. (2012) Structural plasticity of dendritic spines. *Curr. Opin. Neurobiol.* **22,** 383–388
40. Hayashi, Y., and Majewska, A. K. (2005) Dendritic spine geometry: functional implication and regulation. *Neuron.* **46,** 529–532
41. Li, X., Xie, C., Jin, Q., Liu, M., He, Q., Cao, R., Lin, Y., Li, J., Li, Y., Chen, P., and Liang, S. (2009) Proteomic screen for multiprotein complexes in synaptic plasma membrane from rat hippocampus by blue native gel electrophoresis and tandem mass spectrometry. *J. Proteome Res.* **8,** 3475–3486
42. Olsen, J. V., Nielsen, P. A., Andersen, J. R., Mann, M., and Wiśniewski, J. R. (2007) Quantitative proteomic profiling of membrane proteins from the mouse brain cortex, hippocampus, and cerebellum using the HysTag reagent: mapping of neurotransmitter receptors and ion channels. *Brain Res.* **1134,** 95–106
43. Stella, R., Cifani, P., Peggion, C., Hansson, K., Lazzari, C., Bendz, M., Levander, F., Sorgato, M. C., Bertoli, A., and James, P. (2012) Relative quantification of membrane proteins in wild-type and prion protein (PrP)-knockout cerebellar granule neurons. *J. Proteome Res.* **11,** 523–536
44. Chen, P., Li, X., Sun, Y., Liu, Z., Cao, R., He, Q., Wang, M., Xiong, J., Xie, J., Wang, X., and Liang, S. (2006) Proteomic analysis of rat hippocampal plasma membrane: characterization of potential neuronal-specific plasma membrane proteins. *J. Neurochem.* **98,** 1126–1140
45. Dodd, P. R., Hardy, J. A., Oakley, A. E., Edwardson, J. A., Perry, E. K., and Delaunoy, J. P. (1981) A rapid method for preparing synaptosomes: comparison, with alternative procedures. *Brain Res.* **226,** 107–118
46. Chen, C.-H., Wang, S.-M., Yang, S.-H., and Jeng, C.-J. (2005) Role of Thy-1 in in vivo and in vitro neural development and regeneration of dorsal root ganglionic neurons. *J. Cell. Biochem.* **94,** 684–694
47. Maurel, P., Einheber, S., Galinska, J., Thaker, P., Lam, I., Rubin, M. B., Scherer, S. S., Murakami, Y., Gutmann, D. H., and Salzer, J. L. (2007) Nectin-like proteins mediate axon Schwann cell interactions along the internode and are essential for myelination. *J. Cell Biol.* **178,** 861–874
48. Cui, X., Weng, Y.-Q., Frappé, I., Burgess, A., Girão da Cruz, M. T., Schachner, M., and Aubert, I. (2011) The cell adhesion molecule L1 regulates the expression of choline acetyltransferase and the development of septal cholinergic neurons. *Brain Behav.* **1,** 73–86
49. Sakurai, T. (2012) The role of NrCAM in neural development and disorders—beyond a simple glue in the brain. *Mol. Cell. Neurosci.* **49,** 351–363
50. Demyanenko, G. P., Riday, T. T., Tran, T. S., Dalal, J., Darnell, E. P., Brennaman, L. H., Sakurai, T., Grumet, M., Philpot, B. D., and Maness, P. F. (2011) NrCAM deletion causes topographic mistargeting of thalamocortical axons to the visual cortex and disrupts visual acuity. *J. Neurosci.* **31,** 1545–1558
51. Marzban, H., Khanzada, U., Shabir, S., Hawkes, R., Langnaese, K., Smalla, K.-H., Bockers, T. M., Gundelfinger, E. D., Gordon-Weeks, P. R., and Beesley, P. W. (2003) Expression of the immunoglobulin superfamily neuroplastin adhesion molecules in adult and developing mouse cerebellum and their localisation to parasagittal stripes. *J. Comp. Neurol.* **462,** 286–301
52. Munro, M., Akkam, Y., and Curtin, K. D. (2010) Mutational analysis of Drosophila basigin function in the visual system. *Gene* **449,** 50–58
53. Zoghbi, H. Y., and Bear, M. F. (2012) Synaptic dysfunction in neurodevelopmental disorders associated with autism and intellectual disabilities. Cold Spring Harb Perspect Biol 2012;4:a009886
54. Ye, H., Liu, J., and Wu, J. Y. (2010) Cell adhesion molecules and their involvement in autism spectrum disorder. *Neurosignals* **18,** 62–71
55. Melom, J. E., and Littleton, J. T. (2011) Synapse development in health and disease. *Curr. Opin. Genet. Dev.* **21,** 256–261
56. Hussman, J. P., Chung, R. H., Griswold, A. J., Jaworski, J. M., Salyakina, D., Ma, D., Konidari, I., Whitehead, P. L., Vance, J. M., Martin, E. R., Cuccaro, M. L., Gilbert, J. R., Haines, J. L., and Pericak-Vance, M. A. (2011) A noise-reduction GWAS analysis implicates altered regulation of neurite outgrowth and guidance in autism. *Mol. Autism* **2,** 1
57. Pinto, D., Pagnamenta, A. T., Klei, L., Anney, R., Merico, D., Regan, R., Conroy, J., Magalhaes, T. R., Correia, C., Abrahams, B. S., Almeida, J., Bacchelli, E., Bader, G. D., Bailey, A. J., Baird, G., Battaglia, A., Berney, T., Bolshakova, N., Bölte, S., Bolton, P. F., Bourgeron, T., Brennan, S., Brian, J., Bryson, S. E., Carson, A. R., Casallo, G., Casey, J., Chung, B. H., Cochrane, L., Corsello, C., Crawford, E. L., Crossett, A., Cytrynbaum, C., Dawson, G., de Jonge, M., Delorme, R., Drmic, I., Duketis, E., Duque, F., Estes, A., Farrar, P., Fernandez, B. A., Folstein, S. E., Fombonne, E., Freitag, C. M., Gilbert, J., Gillberg, C., Glessner, J. T., Goldberg, J., Green, A., Green, J., Guter, S. J., Hakonarson, H., Heron, E. A., Hill, M., Holt, R., Howe, J. L., Hughes, G., Hus, V., Igliozzi, R., Kim, C., Klauck, S. M., Kolevzon, A., Korvatska, O., Kustanovich, V., Lajonchere C. M., Lamb, J. A., Laskawiec, M., Leboyer, M., Le Couteur, A., Leventhal, B. L., Lionel, A. C., Liu, X. Q., Lord, C., Lotspeich, L., Lund, S. C., Maestrini, E., Mahoney, W., Mantoulan, C., Marshall, C. R., McConachie, H., McDougle, C. J., McGrath, J., McMahon, W. M., Merikangas, A., Migita, O., Minshew, N. J., Mirza, G. K., Munson, J., Nelson, S. F., Noakes, C., Noor, A., Nygren, G., Oliveira, G., Papanikolaou, K., Parr, J. R., Parrini, B., Paton, T., Pickles, A., Pilorge, M., Piven, J., Ponting, C. P., Posey, D. J., Poustka, A., Poustka, F., Prasad, A., Ragoussis, J., Renshaw, K., Rickaby, J., Roberts, W., Roeder, K., Roge, B., Rutter, M. L., Bierut, L. J., Rice, J. P., Salt, J., Sansom, K., Sato, D., Segurado,

R., Sequeira, A. F., Senman, L., Shah, N., Sheffield, V. C., Soorya, L., Sousa, I., Stein, O., Sykes, N., Stoppioni, V., Strawbridge, C., Tancredi, R., Tansey, K., Thiruvahindrapduram, B., Thompson, A. P., Thomson, S., Tryfon, A., Tsiantis, J., Van Engeland, H., Vincent, J. B., Volkmar, F., Wallace, S., Wang, K., Wang, Z., Wassink, T. H., Webber, C., Weksberg, R., Wing, K., Wittemeyer, K., Wood, S., Wu, J., Yaspan, B. L., Zurawiecki, D., Zwaigenbaum, L., Buxbaum, J. D., Cantor, R. M., Cook, E. H., Coon, H., Cuccaro, M. L., Devlin, B., Ennis, S., Gallagher, L., Geschwind, D. H., Gill, M., Haines, J. L., Hallmayer, J., Miller, J., Monaco, A. P., Nurnberger, J. I., Jr., Paterson, A. D., Pericak-Vance, M. A., Schellenberg, G. D., Szatmari, P., Vicente, A. M., Vieland, V. J., Wijsman, E. M., Scherer, S. W., Sutcliffe, J. S., and Betancur, C. (2010) Functional impact of global rare copy number variation in autism spectrum disorders. *Nature* **466,** 368–372

58. Michaelson, J. J., Shi, Y., Gujral, M., Zheng, H., Malhotra, D., Jin, X., Jian, M., Liu, G., Greer, D., Bhandari, A., Wu, W., Corominas, R., Peoples, A., Koren, A., Gore, A., Kang, S., Lin, G. N., Estabillo, J., Gadomski, T., Singh, B., Zhang, K., Akshoomoff, N., Corsello, C., McCarroll, S., Iakoucheva, L. M., Li, Y., Wang, J., and Sebat, J. (2012) Whole-genome sequencing in autism identifies hot spots for de novo germline mutation. *Cell* **151,** 1431–1442
59. Miyata, S., Matsumoto, N., Taguchi, K., Akagi, A., Iino, T., Funatsu, N., and Maekawa, S. (2003) Biochemical and ultrastructural analyses of IgLON cell adhesion molecules, Kilon and OBCAM in the rat brain. *Neuroscience* **117,** 645–658
60. Yuste, R., and Tank, D. W. (1996) Dendritic integration in mammalian neurons, a century after Cajal. *Neuron* **16,** 701–716
61. Connors, B. W., and Regehr, W. G. (1996) Neuronal firing: does function follow form? *Curr. Biol.* **6,** 1560–1562
62. Vissers, M. E., Cohen, M. X., and Geurts, H. M. (2012) Brain connectivity and high functioning autism: a promising path of research that needs refined models, methodological convergence, and stronger behavioral links. *Neurosci. Biobehav. Rev.* **36,** 604–625
63. Penzes, P., Cahill, M. E., Jones, K. A., VanLeeuwen, J.-E., and Woolfrey, K. M. (2011) Dendritic spine pathology in neuropsychiatric disorders. *Nat. Neurosci.* **14,** 285–293
64. Baudouin, S. J., Gaudias, J., Gerharz, S., Hatstatt, L., Zhou, K., Punnakkal, P., Tanaka, K. F., Spooren, W., Hen, R., De Zeeuw, C. I., Vogt, K., and Scheiffele, P. (2012) Shared synaptic pathophysiology in syndromic and nonsyndromic rodent models of autism. *Science* **338,** 128–132
65. Bailey, A., Luthert, P., Dean, A., Harding, B., Janota, I., Montgomery, M., Rutter, M., and Lantos, P. (1998) A clinicopathological study of autism. *Brain* **121 (Pt 5),** 889–905